Synergist Effects of Atomic Oxygen and Ultraviolet Radiation Exposure on Various Spacecraft Materials

A Senior Project

presented to

the Faculty of the Aerospace Engineering Department

California Polytechnic State University, San Luis Obispo

In Partial Fulfillment

of the Requirements for the Degree

Bachelor of Science

by

Adrian L. Doan

14 June, 2013

Synergistic Effects of Atomic Oxygen and Ultraviolet Radiation Exposure on Various Spacecraft Materials

Adrian L. Doan[1]
California Polytechnic State University, San Luis Obispo, CA 93407

The Aerospace Engineering Space Environments Laboratory at California Polytechnic State University features a ground-based system capable of generating atomic oxygen (AO) and vacuum ultraviolet (VUV) radiation environments, constructed by Max Glicklin in 2012. Experiments using three different spacecraft materials were conducted to test the individual and synergistic effects of these naturally occurring phenomena. Kapton HN functioned as a means to provide initial validation of the presence of AO and VUV radiation. Kapton HN also functioned as a test-fluence standard during testing of two other materials. These materials included aluminized beta cloth, with the non-aluminized side being tested, and Indium-Tin-Oxide (ITO) coated aluminized Kapton, with the ITO side being tested. Primary test durations were 24 hours, although a 12 hour test was also completed. Most 24 hour tests exhibited AO fluences of approximately 1.1 x 10^{21} atom·cm^{-2}, or roughly equivalent to four months on-orbit at International Space Station altitude. Vacuum ultraviolet exposure was performed at a sun power of 4.5 G, or roughly equivalent to 108 hours on-orbit for a 24 hour test. Material degradation was observed via mass loss measurements, scanning electron microscope (SEM) images, and reflectance measurements using a diffuse spectrometer. For all test conditions described in this report, all three sample types did not experience observable increases or decreases in degradation due to simultaneous exposure to AO and VUV as opposed to single AO exposure. The beta cloth samples performed as expected, with little degradation relative to the Kapton HN samples. The ITO coated samples did not resist degradation as was expected and featured large changes in surface optical properties, despite negligible mass loss. Because the synergistic effects of AO and VUV are known but no synergistic effects were observed outside the margin of error for the measurements, longer test durations are required in order observe the synergistic effects.

Nomenclature

A	=	surface area of test sample, cm^2
d	=	depth of material erosion, cm
E	=	atomic oxygen erosion yield, cm^3·atom^{-1}
F	=	atomic oxygen fluence, atom·cm^{-2}
Δm	=	mass loss of test sample, g
ρ	=	density of test sample, g·cm^{-3}

Acronyms

AO	=	Atomic Oxygen
AOSS	=	Atomic Oxygen Simulation System
ASTM	=	American Society for Testing and Materials
CCP	=	Capacitively Coupled Plasma
DSS	=	Dark Space Shield
ESH	=	Equivalent Sun Hours
ISS	=	International Space Station
ITO	=	Indium-Tin-Oxide
JAXA	=	Japan Aerospace Exploration Agency
JPL	=	Jet Propulsion Laboratory
LDEF	=	Long Duration Exposure Facility
LEO	=	low Earth orbit

[1] Undergraduate, Aerospace Engineering, California Polytechnic State University, 1 Grand Ave.

MAX = Minimum Atmospheric eXperimentation chamber
MEEP = *Mir* Environmental Effects Payload
MISSE = Materials International Space Station Experiment
RF = Radiofrequency
SEM = Scanning Electron Microscope
UV = Ultraviolet
UVRS = Ultraviolet Radiation System
VUV = Vacuum Ultraviolet

I. Introduction

WITHOUT the protection of Earth's atmosphere, spacecraft are subject to unique the problems of the inhospitable space environment. In low-Earth orbit (LEO), spacecraft interact with the electrically neutral environment (often shortened to "neutral environment").[1] Atomic oxygen (AO) is a naturally occurring component of the neutral environment that is formed when diatomic oxygen molecules are dissociated by short-wavelength ultraviolet (UV) radiation.[2] Previous on-orbit experiments, such as the Long Duration Exposure Facility (LDEF), *Mir* Environment Effects Payload (MEEP), and Materials International Space Station Experiment (MISSE), have shown that spacecraft polymer materials degrade and erode away as a result of exposure to AO.[3] By nature of their organic bonds, polymers tend to have higher erosion yields than other materials. Atomic oxygen has sufficient energy to break many of these atomic bonds. Additionally, the exposure to UV radiation also degrades polymer materials by breaking atomic bonds, the effect of which can easily be seen on the ground via the degradation of outdoor plastics. The simultaneous exposure of materials to AO and UV radiation results in synergistic effects that exceed the effects of each individually. The resultant degradation is of particular concern for spacecraft thermal control because onboard materials are typically chosen for their thermo-optical properties, such as emittance and absorptance, which can be greatly altered by surface degradation.[1,4] Surface erosion may also result in weakened materials in thermal blankets, thereby facilitating the occurrence of rips or holes on-orbit. A significant portion of the cost to manufacture a spacecraft is directly related to the design and testing of spacecraft thermal control systems. Companies spend months and millions of dollars testing their flight-ready spacecraft in thermal vacuum chambers to ensure that the spacecraft can still function in the extreme temperatures of space. Individual components can also be tested under thermal vacuum. Without proper thermal control, spacecraft components could easily drop below or exceed their survivable temperature range. In order to ensure that the spacecraft thermal subsystem will still be functioning throughout the spacecraft mission life, the operational environment and end-of-life characteristics of thermal components must be understood. This is especially important for long-duration missions, where thermal components have a more time to degrade.

Environmental testing is no easy task for the space industry, however. The advent of the NASA Space Shuttle and its ability to both deploy and return satellites facilitated the process of testing materials on-orbit and returning them to the ground for evaluation, such as the LDEF and MISSE experiments. But, the cost to launch and retrieve materials from space is very high, and as of 2011, the Space Shuttle fleet has been retired. As such, ground-based simulation of the AO and UV environment is desired. Various facilities have the ability to replicate the AO and UV environment, but an affordable solution for in-house testing at California Polytechnic State University (Cal Poly) was desired. In 2011-2012, while completing his master's thesis at Cal Poly, Max Glicklin constructed the Minimum Atmospheric eXperimentation (MAX) vacuum chamber and an apparatus capable of subjecting materials to AO and vacuum ultraviolet (VUV) radiation in the Cal Poly Space Environments Laboratory.[4]

Although the presence of AO was previously verified in Ref. [4] using Kapton HN samples, the surface morphology and erosion depth on the samples was not observed. This report presents additional testing of Kapton HN samples using two different exposure times: 24 hours and 12 hours. The synergistic effects of the combined AO and UV environments will be explored via both mass lass and scanning electron microscope (SEM) imagery observations. This report also serves to present the effects of AO and UV radiation exposure on Beta Cloth and Indium-Tin-Oxide (ITO) coated aluminized Kapton. In addition, this report presents lessons learned and instructions for future use of the test equipment originating from unexpected off-nominal operation of the apparatuses. All tests were performed during the Winter 2013 and Spring 2013 quarters at Cal Poly as part of the author's capstone Senior Project, under advisement from Dr. Kira Abercromby in the Aerospace Engineering department.

II. Apparatus

The main components of the test apparatus are the MAX vacuum chamber, the Atomic Oxygen Simulation System (AOSS), and the Ultraviolet Radiation Simulation System (UVRS). The Sample Containment System is directly related to the AOSS, but will be discussed separately.

Both the American Society for Testing and Materials (ASTM) E2089 standard and the *Protocol for Atomic Oxygen Testing of Materials in Ground-Based Facilities* by NASA's Jet Propulsion Laboratory (JPL) calls for Kapton H or Kapton HN polyimide to be used as an AO test-fluence standard.[5,6] Specifically, Kapton H should be used where AO fluences are greater than 2 x 10^{21} atom·cm^{-2}, while Kapton HN can be used at fluences lower than the stated value. This difference is caused by the existence of inorganic particles in Kapton HN that protect the underlying polyimide from AO erosion which would result in inaccurate AO fluence prediction.[5] Previous experiments using the MAX AOGS have yielded fluences less than 2 x 10^{21} atom·cm^{2}, so Kapton HN may be used as a test-fluence standard using these apparatuses. Specifically, Kapton 500HN samples function as the test-fluence standard for the tests described in this report.

A. Vacuum Chamber

A vacuum diagram of the MAX chamber as used in these tests is shown in fig. 1 below. The MAX vacuum chamber is constructed using an approximately 32 cm height x 50 cm diameter STG pyrex cylinder, upper and lower stainless steel endplates, and Varian 600DS Dry Scroll Pump. The upper endplate is removed from the chamber via a pneumatic hoist system. The upper endplate has the capability to support various vacuum feed-throughs, such as an electrical feed-through for RF input for the AOSS (to be described later) and a port to send power and cooling air to the UVRS. The lower endplate is rigidly attached to a large support frame. The lower endplate also has various capabilities for vacuum feed-throughs. These tests make use of a single gas feed-through and thermocouple feed-throughs on the lower end plate.

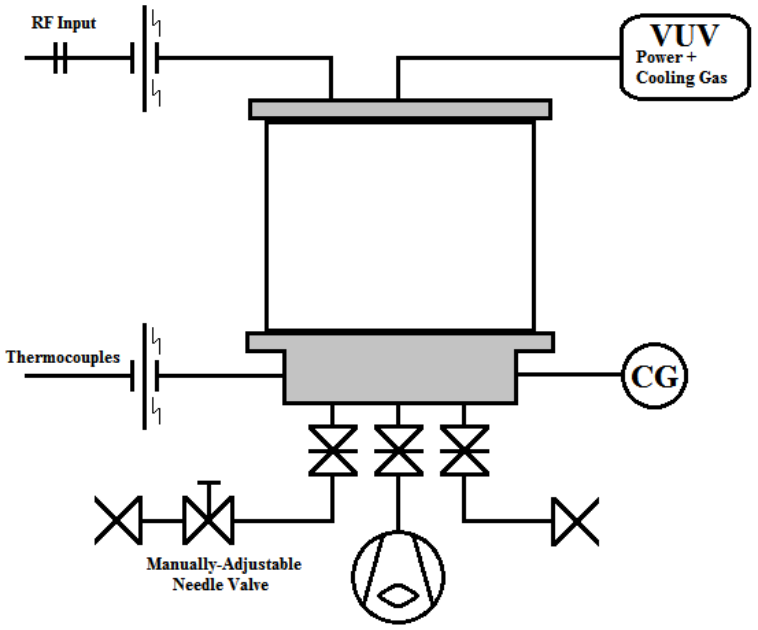

Figure 1. MAX Chamber Vacuum Diagram.

The MAX chamber has capabilities to further reduce chamber pressure via cryogenic pump; however, these capabilities were not needed for this project and thus the hardware for these capabilities are not included on this vacuum diagram.

The Varian Dry Scroll Pump is ideal for atomic oxygen applications, due to its lack of lubricating oil. When coupled with atomic oxygen generating systems, oiled vacuum pumps must use oil that is nonreactive with atomic oxygen. Some of the drawbacks behind using a dry scroll pump, however, are higher base pressures and increased noise output than oiled pumps such as Welch rotary vane mechanical pumps. For this experiment, these drawbacks

were of little concern. Using only the Varian scroll pump, the MAX chamber is capable of achieving pressures of less than 30 mTorr, which is well below the required pressures for the experiments described in this report (to be described later). The chamber also has capabilities to reach lower pressures using a cryopump; however these capabilities were not needed for these tests. The internal chamber pressure can be adjusted manually via opening of a Swagelok cutoff valve and adjustment of a Swagelok needle valve. This input air line flows directly to the sample containment plate inside the chamber, ensuring that the high density of plasma, and thus high density of AO, occurs directly above the samples. Although air has a high volume of nitrogen molecules (N_2), nitrogen has been previously found to have little effect on material degradation.[4] The pressure is monitored via a single InstruTech CVG101GA convectron gauge and a Granville-Phillips 316 vacuum controller.

B. Sample Containment System

Inside the chamber, material samples are exposed to AO in between an RF electrode and a grounding plate, which also serves as the sample containment plate. The sample containment plate is capable of holding four (4) 2"x2" material samples. The exposure area of each sample is controlled via a polished aluminum witness plate with four similarly sized holes. The diameter of these holes is 2.540+/-0.003 cm resulting in an exposure area of 5.06 +/- 0.02 cm^2.[4] The sample containment plate also features a small hole for the input air for the plasma, as described above. The temperature of the sample containment plate is measured via two thermocouples on the underside of the plate. An exploded-view schematic of the sample containment plate is shown below in fig. 2. The exposure areas are the large cutouts in the plate, surrounded by smaller bolt holes.

In general, sample erosion efficiency increases with temperature. In order to ensure normal erosion efficiencies as would be seen during space flight conditions, the temperature of the ground plate was monitored via two thermocouples: one near the center of the plate, and one near the edge of the plate. Instructions in Ref. [4] designate a temperature of 100°C for either of these locations as the maximum acceptable temperature during testing. Measurement of a temperature higher than 100°C necessitates a manual shutdown of the entire system. Monitoring of the ground plate temperature not only ensures that erosion efficiency remains nominal, but also that sputtering of material does not occur due to excess heat.

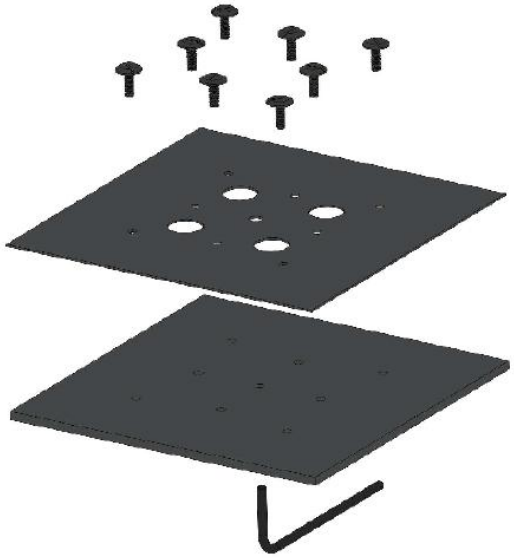

Figure 2. Diagram of the Sample Containment Plate.[4]

C. Atomic Oxygen Simulation System (AOSS)

The AOSS uses RF power to create a capacitively coupled plasma (CCP). Specifically, a Seren R301 operating at 13.56 MHz provides the source of RF power. The power is routed to a Seren AT3 Matching Network, which features both fixed and adjustable capacitors and inductors. These capacitors and inductors can be adjusted either manually or automatically via the Seren MC2 controller. RF power is routed via RG393 cable and a copper feed-through to an aluminum RF electrode inside the MAX vacuum chamber. The plasma occurs between this RF electrode and an aluminum grounding plate at the bottom end of the chamber. The RF electrode is a 15.25 cm diameter, 0.9 cm thick 6061 Aluminum allow disk. The material was chosen for its high resistance to sputtering, thereby reducing possible contamination of the test samples.[4]

The RF electrode is surrounded by an aluminum Dark Space Shield (DSS), grounded to the chamber top end plate via 2 inch solid copper ground strap. The DSS reduces secondary emissions by the RF electrode, ensuring that the primary concentration of plasma is directly above the samples. A description of the design process for the Dark Space Shield is available on pages 30-31 of Ref. [4].

Similar to the DSS, the ground plate (sample containment plate) is grounded to the bottom end plate via 2 inch solid copper ground strap. The gap distance between the RF electrode and the grounding plate is adjustable;

however testing described in Ref. [4] determined that the optimum distance was 7.62 cm based on both sample containment plate temperatures and effective AO flux. The distance was maintained at 7.62 cm for the tests described in this report. An electrical block diagram of the AOSS is shown in fig. 3.

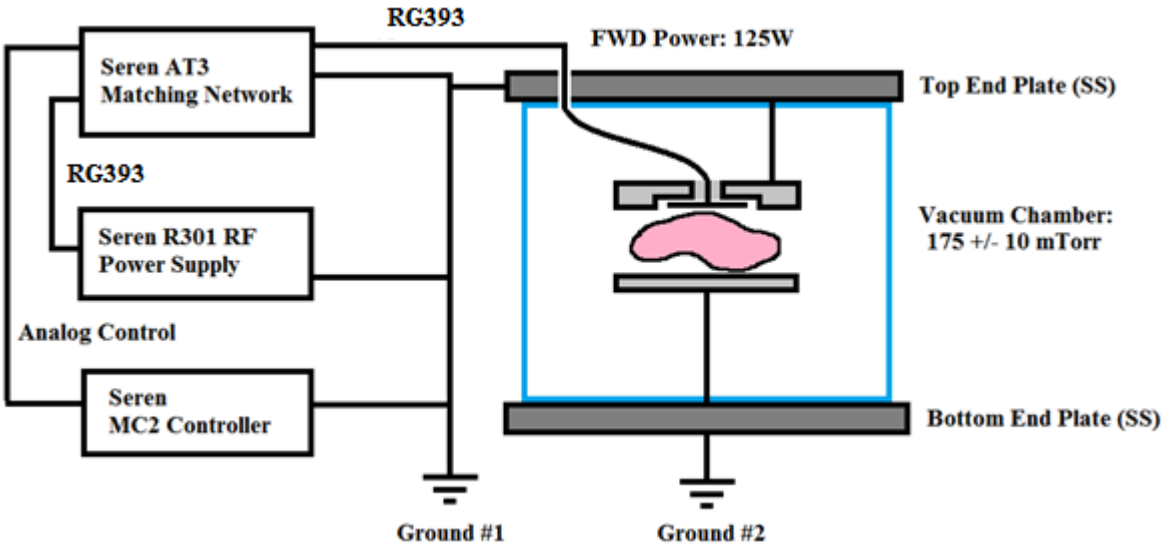

Figure 3. AOSS Electrical Block Diagram.

The Seren AT3 Matching Network either automatically or manually matches system impedance (inductance and capacitance) in order to minimize the RF power that is reflected back into the RF power supply. Nominal testing conditions require 0W of reflected RF power. The AT3 Matching Network is controlled via the Seren MC2 controller. The MC2 detects system impedance and sends control signals to servos within the AT3 Matching Network which rotate variable inductors and capacitors in order to match the system impedance, thereby maximizing forward RF power. In addition to the variable inductors and capacitors, fixed inductors and capacitors can be adjusted by opening up the AT3. This should only be performed if the AT3 is reaching its maximum variable inductance and capacitance limits. These system controls translate to Tune and Load on the MC2 visual readout, given as percentages of the maximum variability. The effective adjustable range is approximately between 5% - 95%. Requiring a Tune or Load above or below this range necessitates opening of the AT3 to adjust the fixed capacitors and inductors.

In order to minimize the leakage of RF into the surrounding environment, the exposed feed-through was covered in Teflon tubing, wrapped with several layers of Kapton tape, and either covered with several layers of Aluminum tape or by an aluminum canister, both of which would be grounded to the chamber top end plate. Similarly, the cable inside the vacuum chamber, which did not have the same internal braiding of a full RG393 cable but still had its Teflon shielding, was wrapped with several layers of aluminum tape to prevent RF leakage. Areas of exposed connections were again shielded with Teflon tubing, wrapped with Kapton tape, and also covered in aluminum tape. The minimization of tapes used in the chamber is desired because the adhesives on the tape may outgas and contaminate samples. However, sufficient tape is necessary to prevent the leakage of RF.

All components of the system were previously designed or chosen to allow 0W reflected power. For example, 2 inch wide copper straps were used as grounding straps because RF travels most efficiently across large widths.[4] In addition to the AT3 Matching Network, ensuring 0W reflected power requires the entire system to be properly tuned. This includes the cleanliness of the copper ground straps, as well as the amount of aluminum tape used to prevent RF leakage through the input power cable.

The copper feed-through for the RF input may require future improvement for this system. The RG393 cable leading up to this feed-through is separated into its main axial core and the protective grounding braid. The main core feeds to the copper feed-through, while the grounding braid attaches to a pair of flexible grounding straps, which then ground to the chamber top end plate. Because the feed-through is constructed using regular copper wire, the connections at this point may be a source of large line losses. A more robust system would consist of a N-Type coaxial connection feed-through.

D. Ultraviolet Radiation Simulation System (UVRS)

The UVRS is composed of a Hamamatsu L10706 Vacuum Ultraviolet (VUV) Light Source, which extends through a flexible bellow from a KF flange. The light source uses a deuterium lamp and a MgF_2 window to allow transmission of light with wavelengths of 115nm or greater.[4] An image of the lamp and its spectral distribution is shown in figures 4 and 5. As can be seen in fig. 5, the lamp outputs between a wavelength of approximately 120-200 nm, which is within the VUV range of 100-200 nm.[4] Although the VUV regime is only a small portion of the total solar output (0.104/1366.1 $W \cdot m^{-2}$), it was selected due to its shorter wavelength, and thus a more energetic photon that is capable of breaking a stronger chemical bond. The full selection process for the lamp is described in detail in Ref. [4].

Due to the geometry of the AOSS, the VUV light source cannot be placed directly above the sample of interest. Because of this, restriction, the lamp is oriented at a 45 degree angle, outside of the AOSS. The distance of the lamp from the sample containment area of interest was determined in Ref. [4] to be 10.72 cm in order to have an effective output on the sample of 4.5 equivalent suns (G), based on a recommended sun power of 3-5G.[4] Thus, a 24 hour test exposure would be equivalent to 108 equivalent sun hours (ESH).

Figure 4. Hamamatsu L10706 VUV Light Source.[7]

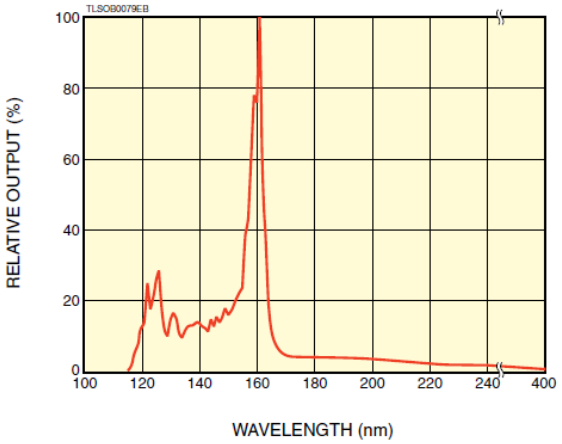

Figure 5. Hamamatsu L10706 Spectral Distribution.[7]

E. Complete Apparatus

A photograph of the entire completed AOSS and UVRS installed in the MAX chamber is shown in fig. 5. A photograph of the system during normal operation is shown in fig. 6.

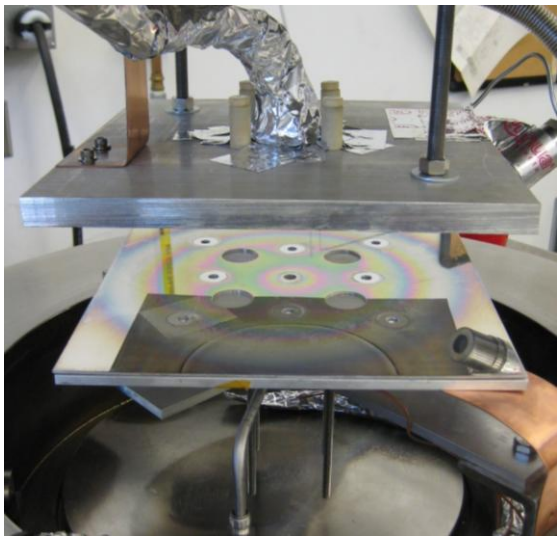

Figure 5. MAX Chamber, AOSS, and UVRS.

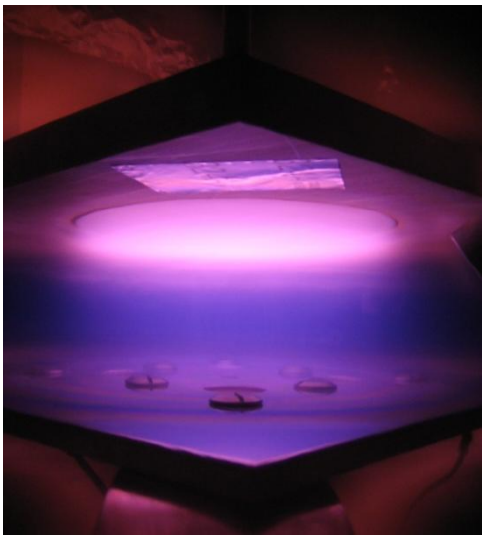

Figure 6. Plasma Formation During Operation.

III. Procedure

The procedure for these tests consists of three major components: Sample dehydration and weighing, sample placement into the chamber and pumping down of the chamber, and initialization of the RF power and UV light source. Initialization of RF power includes tuning of the system in order to achieve optimal testing conditions. The materials that were tested were DuPont Kapton 500HN, Sheldahl aluminized beta cloth with the non-aluminized side being exposed, and Multek Indium-Tin-Oxide (ITO) coated Kapton with aluminized backing, with the ITO surface being exposed. The types of materials used in these tests, as well as their manufacturer's part numbers, are listed in table 1. All materials were donated by Sheldahl brand.

Table 1. Materials Used for Atomic Oyxgen and UV Testing.

Material	Manufacturer	Part Number
Kapton 500HN (5.0 mil)	DuPont	165446-003
Aluminized Beta Cloth	Sheldahl	146626-001
ITO x Kapton (2.0 mil) x Aluminum	Multek	146633-003

Because the aluminized surface of the beta cloth was not directly exposed to AO, the samples will be simply referred to as beta cloth samples. Similarly, ITO-coated Kapton with aluminized backing will simply be referred to as ITO samples. A diagram of the ITO samples is shown in fig. 7. The polyimide layer is 2 mil thick.

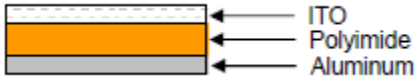

Figure 7. Diagram of ITO-Coated Kapton with Aluminized Backing.[8]

A. Initial Sample Dehydration and Weighing

All materials utilized in these tests were handled using latex gloves to avoid contaminating the samples. Any surfaces that would come into contact with the materials were cleaned with isopropyl alcohol and KIMTECH wipes. The materials were cut into approximately 2 in x 2 in square samples. The samples were dehydrated for a minimum of 48 hours at pressures below 200 mTorr, in accordance with the procedure described in Max Glicklin's thesis and the ASTM E2089 standard.[4,5] The dehydrated samples were then weighed within 5 minutes of removal from vacuum, also in accordance with ASTM E2089.[5] Each sample was weighed a total of five times on a VeriTas S213 scale with a readability of 0.001g and a repeatability of 0.0005g. The masses were then averaged for each sample. The uncertainty of the mass measurements was assumed to be the standard deviation of the sample measurements.

Multiple samples were dehydrated simultaneously in the same vacuum chamber. In order to retrieve new samples for weighing and testing, the chamber was opened and quickly pumped back down to below 200 mTorr. Such a procedure was found in previous tests by NASA to sufficient in avoiding adverse effects on dehydration of the samples.[9]

B. Sample Placement and Chamber Pressure

After being weighed post-dehydration, the samples were placed onto the sample containment plate, with the numbering scheme shown in fig. 8. Only one sample (position #1) received both AO and UV exposure per test, while three other samples were exposed to only AO. As described previously in the Apparatus section, a Kapton HN witness sample was always included in the test, exposed only to AO in order to determine the effective AO flux of the test, following the recommendation of ASTM E2089 and JPL's protocols.[5,6] The Kapton HN witness sample was placed in position 4 in fig. 8 and is deemed the "validation sample". In addition to the validation sample, samples in position 2 and 3 are also only exposed to AO. Position #2 was reserved for a sample of the same material as that in position #1 in order to determine the AO-only effects. Position #3 was reserved for a Kapton HN sample for additional AO validation.

Once the samples were placed in their respective position, the polished aluminum sample cover plate was evenly and snugly bolted to the grounding plate to ensure that each sample's exposure area was confined to the cutout area on the sample cover plate. The MAX chamber was then sealed and the Varian scroll pump was turned on. A Swagelok needle valve was connected to the AOSS gas feed, and the Swagelok cutoff valve blocking the gas feed was then opened completely. The needle valve was adjusted until a chamber pressure of 175 ± 10 mTorr was established, in accordance with instructions for the apparatus.[4]

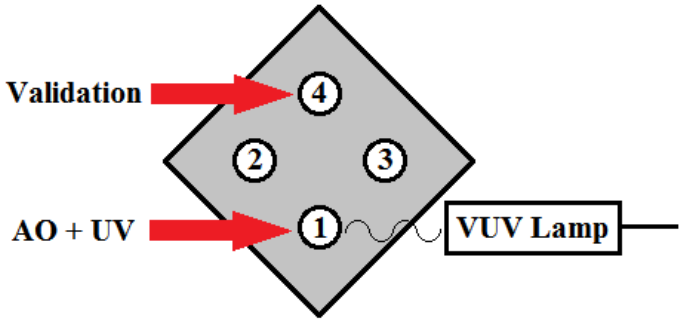

Figure 8. Sample Numbering Scheme.
Note: Not to Scale. Samples 2-4 receive only AO exposure.

C. RF Power and VUV Lamp

While the chamber was pumping down to 175 ± 10 mTorr, the RF input (RG393 co-axial cable) for the AOSS was connected to the Seren AT3 and the air supply hose for UVRS was connected to a facility air supply source. The cooling air supply for the UVRS was then initiated prior to turning on any RF components.

The Seren R301 and Seren MC2 of the AOSS were turned on and the forward RF power was set to 125W on the R301. Although Ref. [4] described the Tune and Load starts points to be set at 50% each, these start points varied from test to test and the system impedance changed over time with repeated use and/or small modifications, such as the addition of more aluminum tape to the RF power lines. Occasionally, the system would require manual tuning in order to match the impedance after the RF power was already turned on. During this tunig time, there was occasionally a smalla mount of reflected power, thereby limiting the forward feed power. In general, the amount of time required for this tuning process was only a small fraction of the overall test time, and this was not considered to be time subtracted from the total exposure time. If occurrence of reflected power above 0W could not be mitigated within 10-20 minutes, then the test was abandoned until the apparatus could be fixed.

Assuming nominal testing conditions, the RF power was initiated and the UVRS was turned on immediately afterward. The cooling air supply for the VUV light source was initiated either before or directly after the lamp was turned on. During testing, operation of the AOSS and UVRS was performed following instructions in Ref. [4]. As described in the apparatus section, the temperature of the sample containment/grounding plate was monitored. A temperature in excess of 100°C would have resulted in a manual shut-down of the test – but, this did not occur during any of the testing described in this report. The system was monitored on an approximately hourly basis by the author of this report, except during 24 hour tests when a small amount of sleep was required. This monitoring included monitoring of chamber pressure, sample containment plate temperatures, vacuum pump temperature, reflected RF power, Tune, Load, forward DC voltage, phase, and magnitude of the system. If reflected power above 0W was recorded and could not be reduced back to 0W via adjustment of the Tune, Load, Phase, and/or Magnitude, then the test was abandoned.

D. System Shut-Down and Final Sample Weighing

At the completion of the test, the RF power was ceased and all Seren components turned off to prevent accidental initiation of RF power. The VUV lamp was simultaneously turned off. The cooling air supply for the VUV lamp was left running until the samples were ready to be removed. In order to remove the samples, the chamber was left under vacuum for several hours below 200 mTorr to prevent re-gassing of the samples while the sample containment plate reached acceptable temperatures to be handled by hand. Once the temperature of the sample containment plate had decreased to lower than approximately 40°C, the chamber was vented and samples removed for weighing. Weighing was completed within 5 minutes of their removal from vacuum in accordance with ASTM E2089.[5]

E. Sample Storage and Scanning Electron Microscope Observations

After testing, samples were separately wrapped in a KIMTECH wipes, then stored in separate zip-seal plastic bags. Ideally, the samples would be stored under vacuum, with no surfaces touching the area of interest, up until SEM testing would be performed. Restrictions on the use of laboratory vacuum chambers did not allow for this, however.

Samples of interest were given to Dr. Harding of the Cal Poly Materials Engineering (MATE) department for SEM imaging. The SEM images were then given back to the author, who performed erosion depth analysis using the images.

F. Spectrometer Observations

After the samples had been observed in the SEM by the MATE department, they were then given to Dr. Abercromby for reflectance measurements using an ASD FieldSpec spectrometer. The spectrometer has 717 channels and a bandwidth of 10nm at 2 microns. The diffuse reflectance of each sample from 350 – 2500 nm was measured three times in both the exposed area and the non-exposed area.

Diffuse reflectance was recorded at approximately 90 degrees from the source, except for the ITO samples. Because the ITO samples have a high spectral reflectance, the spectrometer was positioned outside of this nominal position, in order to avoid over saturating the sensor with the spectral reflection. This then measures the diffuse reflection.

IV. Analysis

Ground-based simulation of the AO environment can fall into two categories: low energy (0.1 eV) isotropic thermal plasmas to higher energy (70 eV) hyperthermal directed plasmas. Low energy, isotropic AO plasmas consist of low speed AO atoms traveling in all directions, as opposed to the high speed, directional atoms associated with high energy, directed plasmas. Directed, high energy plasmas better simulate the AO found in LEO due to the high orbital speed of spacecraft at LEO altitudes. The erosion caused by high speed, directed AO atoms can be somewhat replicated by a higher density of low energy AO atoms, which can be created using lower-cost solutions than with high energy plasmas.[4] Max Glicklin constructed the AOSS to use RF power in order to create low energy, capacitively coupled plasma (CCP) between two RF electrode plates. The AO created by this system has an energy between ~0.04 – 0.1 eV, as opposed to the orbital AO energy of 4.5 eV.[4] This means that the apparatus described in this report should not be capable of creating the tall cones and pits in the eroded area that are seen during orbital exposures.[4]

Vacuum ultraviolet (VUV) is defined to be within the range of 100-200 nm wavelengths. The solar flux of this region alone is 0.104 $W \cdot m^{-2}$. The effective AO fluence of ground-based systems can be found using the mass lost by Kapton witness samples. Using erosion yields and material densities found in previous experiments, the effective fluence in $atom \cdot cm^{-2}$ can be found by

$$F = \frac{\Delta m}{EA\rho} \tag{1}$$

where Δm is the mass loss of the material after exposure, E is the material's erosion yield in $cm^3 \cdot atom^{-1}$, A is the exposure area in cm^2, and ρ is the density of the material in $g \cdot cm^{-3}$.[2] Material erosion yield values vary between previous space-based experiments, so multiple values of erosion yields should be considered. For this experiment, the exposure area A is assumed to be 5.06 +/- 0.02 cm^2.[4]

The relationship between erosion depth, material properties, and fluence is

$$d = \frac{\Delta m}{A\rho} = EF \tag{2}$$

where d is the erosion depth in cm.[2] Again, the erosion yield E of Kapton HN varies depending on the source. Kapton HN as part of MISSE were found to have an AO erosion yield of 2.81 x 10^{-24} $cm^3 \cdot atom^{-1}$.[3,9] ASTM E2089 lists the erosion yield for Kapton H or HN to be 3.0 x 10^{-24} $cm^3 \cdot atom^{-1}$.[5] The erosion depth can be determined via analysis of SEM images. Given a known scale of the SEM images, the erosion depth is measured by determining the pixel length between two pixel points: one at the edge of the unexposed area, and one at the bottom of the exposed area. This pixel length is then related to the known scale in order to determine a true length. If the image was taken at a 45 degree angle, then simple geometry allows the vertical height of the erosion depth to be determined by dividing the calculated length by $\sqrt{2}$.

The density of Kapton HN can be found utilizing data from DuPont. Specifically, the average density and the error in this density can be calculated from the maximum and minimum possible densities based on film thickness and mass per unit area. The maximum possible density is

$$\rho_{max} = \frac{Max\ Unit\ Weight}{Min\ Thickness}, \tag{3}$$

and the minimum possible density is

$$\rho_{min} = \frac{Min\ Unit\ Weight}{Max\ Thickness}, \tag{4}$$

where density is in g·cm^{-3}, unit weight is in g·cm^{-2}, and thickness is in cm. The average density is then calculated as

$$\rho_{avg} = \frac{\rho_{max}+\rho_{min}}{2}. \tag{5}$$

The uncertainty in mass loss was calculated by summing the uncertainty of the initial mass with the uncertainty of the final mass. These uncertainties were determined by finding the standard deviation of five separate measurements for each sample. The uncertainty in the density will be defined to be

$$\delta\rho = \rho_{max} - \rho_{avg}, \tag{6}$$

The uncertainty in fluence values, δF, was determined by summing the absolute values of the partial derivates of each component in equ. (1), or

$$\delta F = \left|\frac{\partial \mathrm{F}}{\partial \Delta \mathrm{m}}\right| \delta\Delta m + \left|\frac{\partial \mathrm{F}}{\partial \mathrm{A}}\right| \delta A + \left|\frac{\partial \mathrm{F}}{\partial \mathrm{E}}\right| \delta E + \left|\frac{\partial \mathrm{F}}{\partial \rho}\right| \delta\rho \tag{7}$$

where δE is assumed to be zero. Given this assumption, the uncertainty in fluence can be calculated by

$$\delta F = \left|\frac{1}{EA\rho}\right| \delta\Delta m + \left|\frac{-\Delta \mathrm{m}}{\mathrm{EA}^2\rho}\right| \delta A + \left|\frac{-\Delta \mathrm{m}}{\mathrm{EA}\rho^2}\right| \delta\rho. \tag{8}$$

V. Results

All testing was completed during the Winter 2013 and Spring 2013 quarters at Cal Poly. All tests were originally planned to be 24 hour tests; however, the high potential for the occurrence of reflected power back into the RF power supply resulted in several 12 hour tests. These 12 hour tests could be monitored by a single student for the majority of the test. Due to budgetary limitations, not all samples described in this report were observed using the SEM. Choice of which samples would be measured in the SEM varied from test to test.

DuPont Kapton500HN was used as the test-fluence standard for all of the exposure tests in this report. The density of Kapton 500HN was found using equations [3] – [6]. The specifications for DuPont Kapton 500 HN are listed in table 2.[10] The specifications listed below result in a density of 1.4388 ± 0.1925 g·cm^{-3}.

Table 2. DuPont Kapton 500HN Specifications.[9]

Nominal Thickness mil (µm)	5.00 (127)
Minimum Thickness mil (µm)	4.65 (118)
Maximum Thickness mil(µm)	5.35 (136)
Minimum Unit Weight g/m^2	169.5
Maximum Unit Weight g/m^2	192.5

A. Preliminary Validation Using Kapton HN

Preliminary validation of the system called for the use of all Kapton HN samples. This allows for the distribution of atomic oxygen across the three non-UV exposed samples to be observed. A photo of a Kapton HN sample exposed to AO for 24 hours is shown in fig. 9. The exposure area is the large, dull circular area in the center of the photo. The unexposed Kapton is the remaining reflective orange surface. A noticeable depth of erosion could be seen with the naked eye. There was no noticeable difference between Kapton HN samples exposed to only AO and those exposed to both AO and UV.

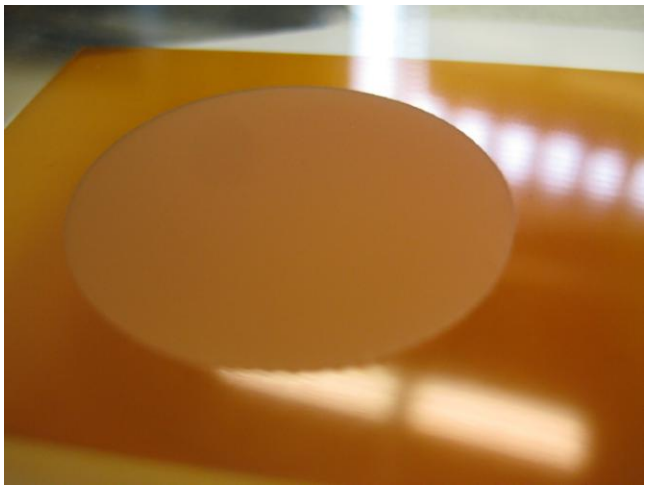

Figure 9. Typical Example of an Exposed Kapton 500HN Sample.

Table 3. Initial Kapton 500 HN 24 Hour Exposure

No.	Sample Type	Exposure	Avg. Initial Mass (g)	Avg. Final Mass (g)	Average Mass Loss (g)
1	Kapton 500HN	AO + UV	0.443 ± 0.001	0.414 ± 0.002	0.029 ± 0.003
2	Kapton 500HN	AO	0.338 ± 0.001	0.313 ± 0.002	0.025 ± 0.003
3	Kapton 500HN	AO	0.394 ± 0.001	0.370 ± 0.001	0.023 ± 0.002
4	Kapton 500HN	Validation	0.432 ± 0.001	0.409 ± 0.001	0.023 ± 0.002
Mass loss Effective AO Fluence			**ASTM E2089**		$1.1 \pm 0.2 \times 10^{21}$ atom·cm^{-2}
			MISSE 2		$1.1 \pm 0.3 \times 10^{21}$ atom·cm^{-2}

The first test completed was a full 24 hour test, the results of which are shown in table 3 above. This test was completed after issues with reflected power had been mitigated. The AO fluence was $1.1 \pm 0.3 \times 10^{21}$ atom·cm^{-2}, using MISSE 2 Kapton HN erosion yield data. This is roughly equivalent to 4 months at the International Space Station (ISS) Orbit, where a full year was expected to be 3.28×10^{21} atom·cm^{-2}.[9]

Using average mass loss, the AO+UV sample had 26% more mass loss than the AO-only validation sample. But, given worst-case measurements, this experiment showed that for a 24 hour test, the mass loss difference between the UV exposed sample and the non-UV validation sample is nearly negligible. This is also the case with the other non-UV samples from this same test. This analysis, however, was not performed until completion of all testing. Early analysis may have revealed the need for longer test durations in order to see a noticeable difference between the UV and non-UV samples.

A subsequent test with beta cloth as the primary sample resulted in the occurrence of reflected power in the system. This necessitated additional tuning of the system to mitigate reflected power. No erosion depth measurements were made using the SEM for this test because another 24 hour Kapton HN test was completed after the system had been readjusted to mitigate reflected RF power. But, based on the mass loss, exposure area, and density, the average erosion depth is expected to be approximately 32 μm for the primary AO-validation sample (sample #4).

Table 4. Kapton 500 HN 24.25 Hour Exposure

No.	Sample Type	Exposure	Avg. Initial Mass (g)	Avg. Final Mass (g)	Average Mass Loss (g)
1	Kapton 500HN	AO + UV	0.381 ± 0.001	0.356 ± 0.001	0.025 ± 0.001
2	Kapton 500HN	AO	0.387 ± 0.001	0.363 ± 0.001	0.024 ± 0.003
3	Kapton 500HN	AO	0.395 ± 0.001	0.364 ± 0.001	0.031 ± 0.003
4	Kapton 500HN	Validation	0.268 ± 0.001	0.242 ± 0.001	0.026 ± 0.002
Mass loss Effective AO Fluence			**ASTM E2089**		$1.2 \pm 0.3 \times 10^{21}$ atom·cm^{-2}
			MISSE 2		$1.3 \pm 0.3 \times 10^{21}$ atom·cm^{-2}

The second 24 hour Kapton HN test also revealed negligible difference between the mass loss of the UV-exposed sample and the AO-only validation sample, as shown in table 4. In fact, one of the other non-UV samples featured higher mass loss than the UV sample. These results are not completely consistent with previous results using the same apparatus, as described in ref. [4]. The previous tests described in ref. [4] show a higher masses loss for AO+UV samples than for singular AO samples just outside the margin of error. AO+UV samples were described as exhibiting 10.1% and 15.4% more mass loss than AO-only samples, based on two separate tests – though, these percentages did not account for worst case measurements and errors.

The immeasurability of a difference for the synergistic effect of AO+UV may be caused by limited VUV output due to a contaminated lamp window, or broken lamp – though, the lamp was purchased brand new by Max Glicklin and had not accumulated enough hours of usage to warrant a lamp failure as a cause. Additionally, the lamp window was visually inspected and was found to be non-obstructive. According to Hiroyuki Shimamura and Eiji Miyazaki of the Japan Aerospace Exploration Agency (JAXA), the lack of a significant difference between AO-only and simultaneous AO+UV exposure could potentially be because the synergistic effects are minimal. Shimamura and Miyazaki found that the simultaneous exposure of polyimide to both AO and VUV in LEO environment conditions did not result in a significant increase in erosion relative to AO-only samples.[11] Key differences between the tests performed by the author of this report and those performed by Shimamura and Miyazaki were the total AO fluence and the ESH. For this 24.25 hour test, there was an ASTM E2089 AO fluence of $1.2 \pm 0.3 \times 10^{21}$ atom·cm^{-2}, while the AO fluence by Shimamura and Miyazaki was $2.7\text{-}3.0 \times 10^{20}$ atom·cm^{-2}, which is more on par with a 6 hour test in the AOSS (2 months on-orbit at ISS altitude). The Shimamura and Miyazaki's ESH, however, was significantly higher than the ESH created by the UVRS. The JAXA experiment utilized a VUV flux of approximately 0.3 mW·cm^{-2}, which equates to a equivalent sun power of 30 G based on the solar VUV flux of 0.104 W·m^{-2}.[11] This is well above the recommended maximum of 5 equivalent suns for test conditions.[4] This means that the results of the JAXA experiment may be potentially distorted due to excess VUV causing unique effects on the sample materials.

Based on mass loss, the expected average erosion depth is approximately 36 μm for the primary AO-validation sample (sample #4) and 33 μm for sample #2. SEM images of sample #1 are in figures 10 and 11 below. Figure 10 shows a view of the exposed and unexposed surfaces of sample #1 at 422x magnification and a 45° view angle. The exposed area features a series of large pits, but no cones. Based on this image, the approximate erosion depth is between 15 – 18 μm, or half the expected depth using the mass loss. The source of this discrepancy is unknown. Figure 11 shows another view of the same sample, with slightly higher magnification. In this image, small cones can be seen on the surface of the eroded area. This image was not used for any erosion depth calculations because the view angle is not known.

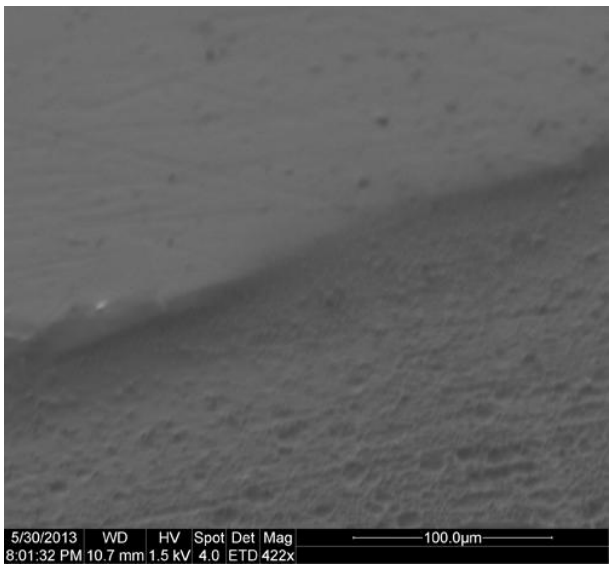

Figure 10. SEM Image of Sample #1– Kapton 500HN 24.25 Hour Test – 422x Magnification. *This image shows the unexposed area (top) and the exposed area (bottom). In this specific section of the sample, both large and small pits have formed, though there is a general lack of cones.*

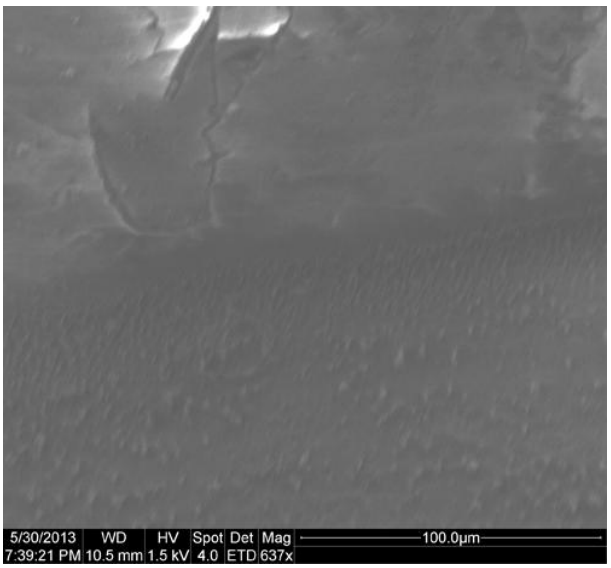

Figure 11. Sample #1 – Kapton 500HN 24.25 Hour Test – 637x Magnification. *Another view of the unexposed area (top) and exposed area (bottom) at 637x Magnification reveals small cones caused by AO+UV degradation.*

Samples #2 and #3, shown in fig. 12 and fig. 13, respectively, do not feature the same cones as those on sample #1, based on the available SEM images. The erosion on sample #3 appears more similar to a series of random "walls" than of individual cones, like those seen in fig. 11. Sample #4, shown with two different views in fig. S4_T6, also features slightly different surface morphology. Because samples #2 - #4 all received AO-only exposure, their surface morphologies should be nearly identical. And, according to Shimamaru and Miyazaki, the surface morphology for AO-only and AO+UV exposed samples should be very similar. Ideally, the location of the SEM images on the samples would be known relative to their orientation in the AOSS. This would allow the distribution of AO across each sample to be observed. The erosion on sample #4, shown in fig. 14 and fig. 15, does not appear strikingly different than on sample #1. The SEM images are only useful on a very local level, however.

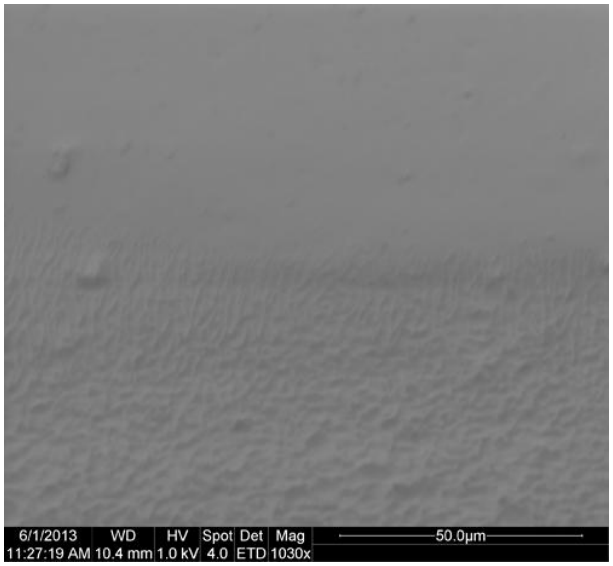

Figure 12. SEM Image of Sample #2 – Kapton 500HN 24.25 Hour Test – 1030x Magnification. *Exposed surfaces are in the bottom half, while unexposed are in the top half of the image.*

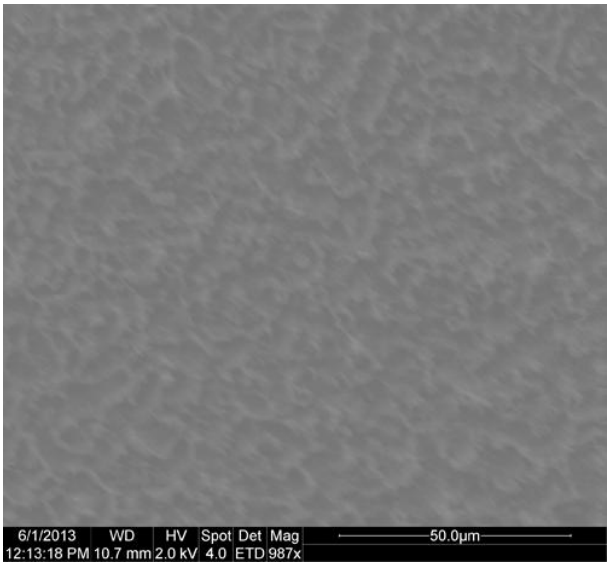

Figure 13. SEM Image of Sample #3 – Kapton 500HN 24.25 Hour Test – 987x Magnification. *This SEM image shows that the eroded surface does not consist of cones, but "walls".*

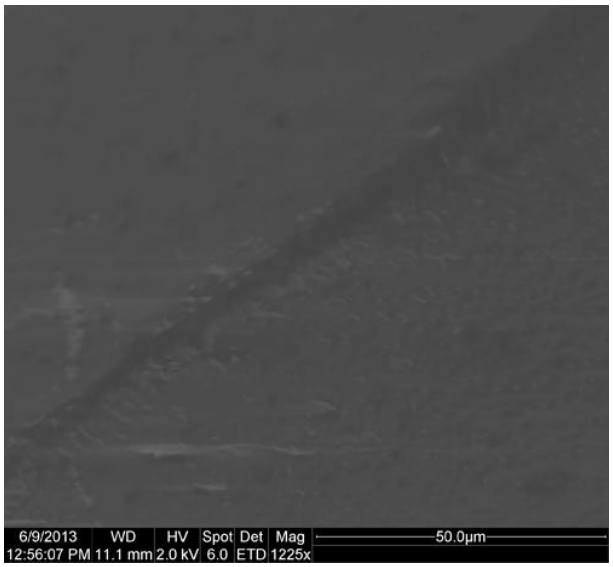

Figure 14. SEM Images of Sample #4 – Kapton 500HN 24.25 Hour Test – 1225x Magnification. *This image mostly shows a series of pits in the eroded area of sample 4, while there is a general lack of small cones.*

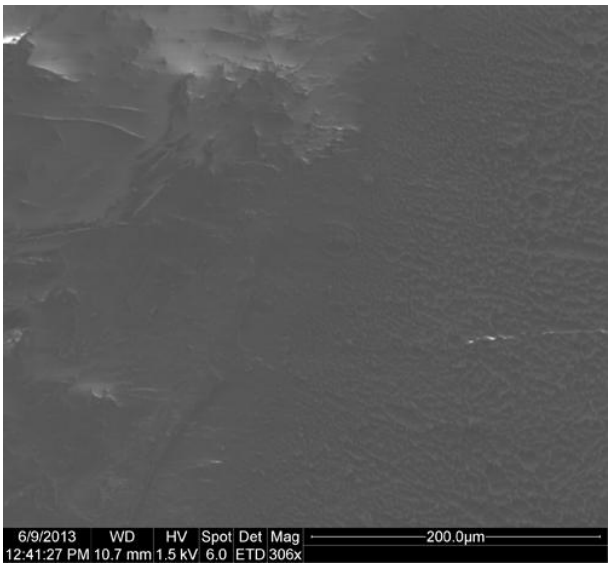

Figure 15. SEM Images of Sample #4 – Kapton 500HN 24.25 Hour Test – 306x Magnification. *This image shows both large pits and small cones in the eroded area of sample 4.*

Additional verification that the AO and AO+UV samples did not feature significantly different erosions is shown via a similar spectral response for the two samples in fig. 16. Prior to exposure, Kapton HN has a relatively smooth surface capable of producing clearly reflected images, thus having a high spectral reflectance, and lower diffuse reflectance. After exposure, the reflectance across wavelengths 350-2500 nm increased by similar amounts for AO and AO+UV samples. The similar increases in diffuse reflectance in this study suggest that there is no significant difference between AO-only and AO+UV exposure, such that the overall surface morphology for AO-exposed and AO+UV exposed polyimide is nearly identical. For both cases, an overall increase in diffuse reflectance of spacecraft materials results in a decrease of spectral reflection of incoming solar energy. Assuming a spacecraft without variable thermal control and at LEO altitude, the spacecraft will run warmer at end-of-life than at beginning-of-life. This relationship must be accounted for in the design of the rest of the thermal subsystem.

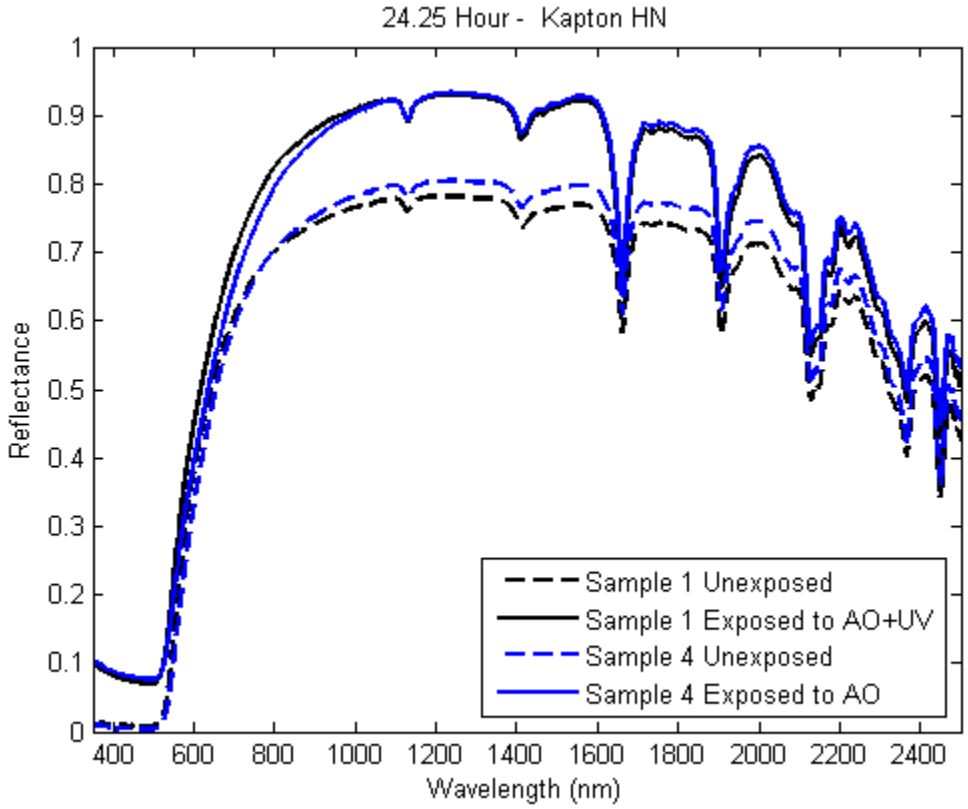

Figure 16. Reflectance Before and After 24.25 Hour AO and AO+UV Exposure on Kapton HN.

Because AO and VUV are both capable of breaking the organic bonds in polymers, synergistic effects should be present. The lack of a difference between individual and synergistic effects results from the short length of the experiment and the magnitude of the error on the mass loss measurements. For this apparatus, 24 hours is not sufficient to show the synergistic effects well outside of the margin of error. Even if there were a 1mg increase in mass loss due to simultaneous exposure, it would not be measurable due to the accuracy of the scale. Also, because the total AO fluence is approximately equivalent to 4 months (2880 hours) in ISS orbit, while the ESH is only 108 hours, future tests should attempt to better replicate the LEO environment. This could be achieved by increasing the gap distance between the RF electrode and the ground plate, or decreasing the forward RF power in order to decrease the AO flux. The VUV lamp is non-adjustable and would remain on for the duration of the test, as is already in the procedure.

Table 5. Kapton 500 HN 12 Hour Exposure

No.	Sample Type	Exposure	Avg. Initial Mass (g)	Avg. Final Mass (g)	Average Mass Loss (g)
1	Kapton 500HN	AO + UV	0.395 ± 0.002	0.382 ± 0.000	0.013 ± 0.002
2	Kapton 500HN	AO	0.397 ± 0.001	0.383 ± 0.001	0.014 ± 0.001
3	Kapton 500HN	AO	0.440 ± 0.001	0.426 ± 0.001	0.014 ± 0.003
4	Kapton 500HN	Validation	0.368 ± 0.000	0.355 ± 0.001	0.013 ± 0.001
Mass loss Effective AO Fluence			**ASTM E2089**	$6.0 \pm 1.3 \times 10^{20}$ atom·cm^{-2}	
			MISSE 2	$6.3 \pm 1.4 \times 10^{20}$ atom·cm^{-2}	

Prior to completing any analysis on the 24.25 hour test samples, a 12 hour test was completed to see if simultaneous AO+UV exposure would result in synergistic effects during this shorter test period. The test yielded similar results to the 24.25 hour test, where AO and AO+UV samples exhibited similar mass losses within the margin of error. Similar to the 24 hour tests, differences between UV and non-UV exposed samples could not be seen by the naked eye for the shorter test duration of 12 hours. Unlike the AO+UV sample from the 24.25 hour test, SEM images of the AO+UV sample in the 12 hour test featured a much higher density of cones in the eroded area, as can been see in figures 17 and 18. Sample #4 (AO only) in the 12 hour test did not feature the same cones and pits as those on sample #1 (AO+UV). As can be seen in figures 19 and 20, the eroded surface on the 4th sample is very smooth, with a few pits scattered on the surface. But, as stated previously, the SEM images only represent a local morphology. In order to look at the overall effects, the spectral response of the two samples was observed using a spectrometer.

Figure 17. SEM Image of Sample #1 – Kapton 500HN 12 Hour Test – 477x Magnification. *This image reveals cones and pits, as well as a small piece of debris (center) that attached itself between AO+UV testing and SEM observations.*

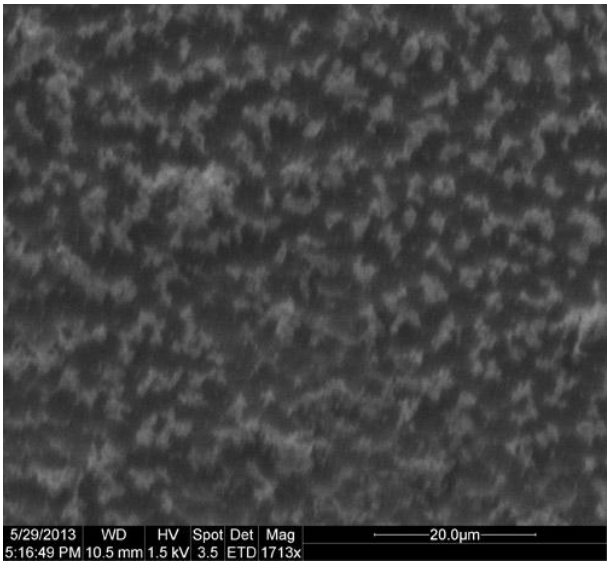

Figure 18. SEM Image of Sample #1 – Kapton 500HN 12 Hour Test – 1713x Magnification. *This image shows a closer view of the cones and pits caused by AO+UV surface degradation.*

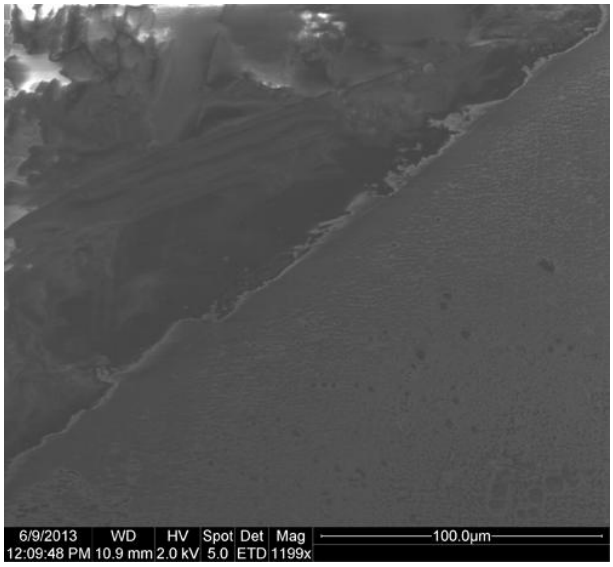

Figure 19. SEM Image of Sample #4 – Kapton 500HN 12 Hour Test – 1199x Magnification. *This high magnification image shows both the eroded surface (lower right corner) as well as the "wall" (upper left corner) between the exposed and unexposed areas. Compared to the AO+UV sample, the eroded surface is relatively smooth.*

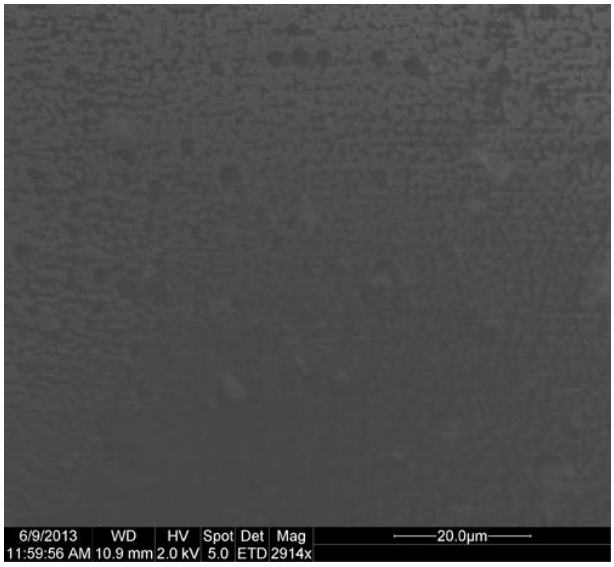

Figure 20. SEM Image of Sample #4 – Kapton 500HN 12 Hour Test – 2914x Magnification. *Higher magnification further reveals the relatively smooth eroded surface when compared to that of the AO+UV exposed Kapton HN sample.*

Figure 21 shows the reflectance for Kapton HN before and after 12 hours of exposure. Although sample #1's control diffuseness (unexposed to AO+UV) was measured to be higher than the control of sample #4, both had similar trends across the 350-2500 nm wavelength range. Additionally, the change in diffuseness for sample #1 and #4 after their respective test exposures was similar, despite the additional presence of UV on sample #1. So, even though the two samples appeared to have very different local surface morphologies in the SEM images, the important factor for thermal control are the optical properties, which are very similar. This is consistent with the 24.25 hour results described above. Being that a 12 hour test duration results in only 54 ESH, the test may be deemed far too short to notice any synergistic effects of AO and UV. Figure 22 shows that for the 24.25 hour test, the increases in diffuseness follow each other closely. For the 12 hour test, the increase in the AO-only sample was higher than the AO+UV sample, which is not expected know that simultaneous exposure should increase degradation. But, this is due to the short test duration, such that the effects do not exceed the system uncertainty.

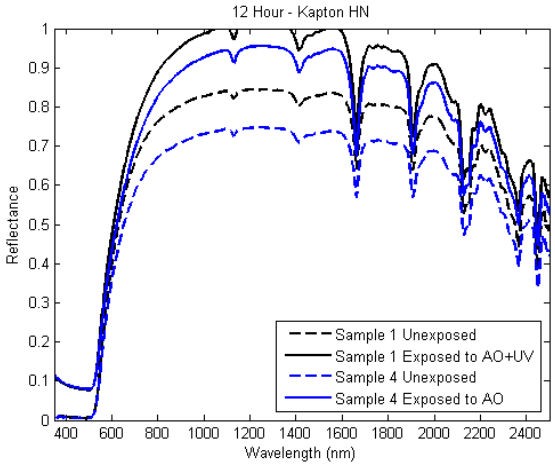

Figure 21. Reflectance Before and After 12 Hour AO and AO+UV Exposure on Kapton HN.

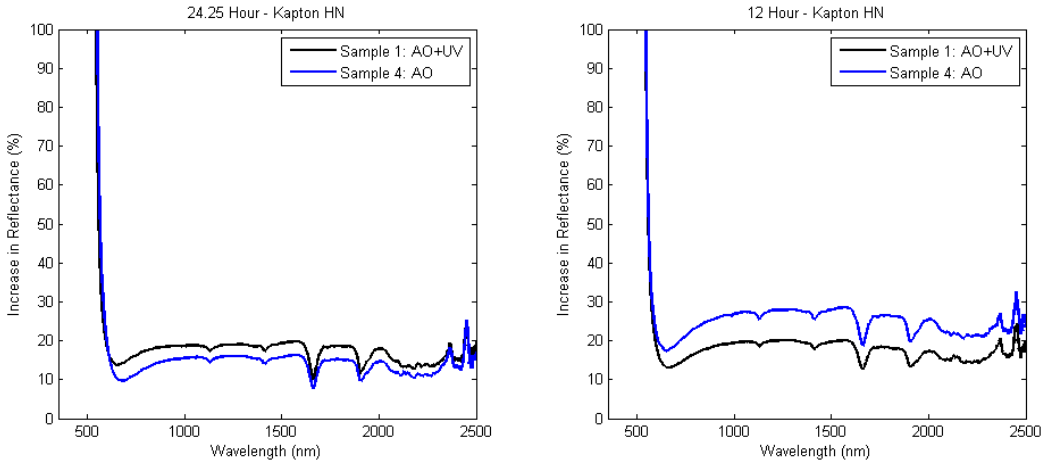

Figure 22. Increase in Reflectance for 24.25 Hour and 12 Hour Exposed Kapton HN.

B. Beta Cloth

Beta cloth is a type of fiberglass woven fabric, not a polymer. As such, the beta cloth was expected to experience less degradation than the Kapton HN witness samples. Naturally an off-white color, darkening of the beta cloth should be expected due to UV degradation.[12] According to experiments described in Ref. 12, Near-UV had more of an effect on beta cloth darkening than VUV. Additionally, the presence of AO countered nearly all of the degradation due to the UV exposure. Degradation was mostly a factor of silicone presence in the beta cloth.[12]

Table 6. Beta Cloth – 12-24 Hour Exposure

No.	Sample Type	Exposure	Avg. Initial Mass (g)	Avg. Final Mass (g)	Average Mass Loss (g)
1	Beta Cloth	AO + UV	0.480 ± 0.002	0.475 ± 0.001	0.006 ± 0.003
2	Beta Cloth	AO	0.500 ± 0.001	0.492 ± 0.001	0.008 ± 0.002
3	Kapton 500HN	AO	0.358 ± 0.001	0.331 ± 0.001	0.027 ± 0.002
4	Kapton 500HN	Validation	0.319 ± 0.002	0.294 ± 0.000	0.025 ± 0.003
Mass loss Effective AO Fluence			**ASTM E2089**	$1.1 \pm 0.3 \times 10^{21}$ atom·cm^{-2}	
			MISSE 2	$1.2 \pm 0.3 \times 10^{21}$ atom·cm^{-2}	

Table 6 shows the results of a beta cloth test that was expected to be 24 hours. However, at some point between 12-24 hours of test duration, the AOSS featured significant reflected power, at least above 10W. This severely limited the forward power, which was set to 125W. Because there was a decrease in forward power in the latter half of the test, there was most likely a non-uniform AO flux throughout the test. But, the overall AO fluence was found to be on par with a regular 24 hour test. Because of this, the test was not considered to be a complete failure. As can be seen in table 6, the beta cloth did experience a small amount of mass loss, though this is most likely due to sputtering of contaminants and/or silicone off the surface of the beta cloth. Figure 23 shows a photograph of beta cloth sample. The exposed area of the beta cloth was a noticeable shade darker than the unexposed area, though there was not a significant change. Although optical and thermo-optical properties for the beta cloth pre- and post-test were not measured in this experiment, Ref. 12 found that there was nearly no change in the properties after simultaneous AO+UV exposure. In fact, it was found that AO countered some if not all of the degradation by UV.[12] Future experiments using the AOSS and UVRS should measure the change in optical properties of the beta cloth.

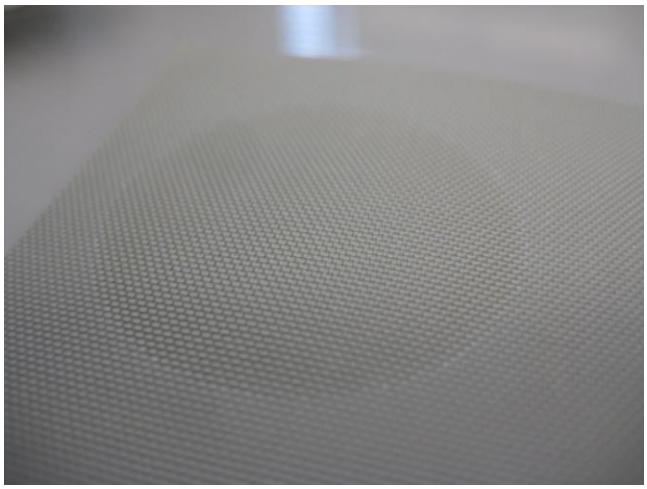

Figure 23. Beta Cloth Sample Exposed to AO and UV.

Table 7. Beta Cloth – 24 Hour Exposure

No.	Sample Type	Exposure	Avg. Initial Mass (g)	Avg. Final Mass (g)	Average Mass Loss (g)
1	Beta Cloth	AO + UV	0.469 ± 0.001	0.461 ± 0.001	0.008 ± 0.002
2	Beta Cloth	AO	0.488 ± 0.001	0.482 ± 0.001	0.006 ± 0.002
3	Kapton 500HN	AO	0.303 ± 0.001	0.288 ± 0.001	0.015 ± 0.002
4	Kapton 500HN	Validation	0.262 ± 0.001	0.249 ± 0.001	0.013 ± 0.002
Mass loss Effective AO Fluence			**ASTM E2089**		$6.0 \pm 1.7 \times 10^{20}$ atom·cm^{-2}
			MISSE 2		$6.3 \pm 1.8 \times 10^{20}$ atom·cm^{-2}

Because the first beta cloth test was a partial failure arising from the occurrence of reflected power in the AOSS, a second test was completed after the system was retuned. During the second beta cloth test, there was a noticeable decrease in the AO flux, based on the Kapton HN witness sample. This may be due to the fact that the non-UV beta cloth sample accidentally made contact with a potentially oily table surface, and was not re-dehydrated after this event. There was also a noticeable surface finish difference on the Kapton witness sample than in all previous tests, as can be seen in fig. 24. Note the large multi-directional etch marks in the center exposure area that are not seen in fig. 9. Additionally, there are some areas of increased erosion depth than other areas. This may have been caused by contamination on the surface of the Kapton HN sample, originating from any oils or other particles that may have adhered to the beta cloth sample.

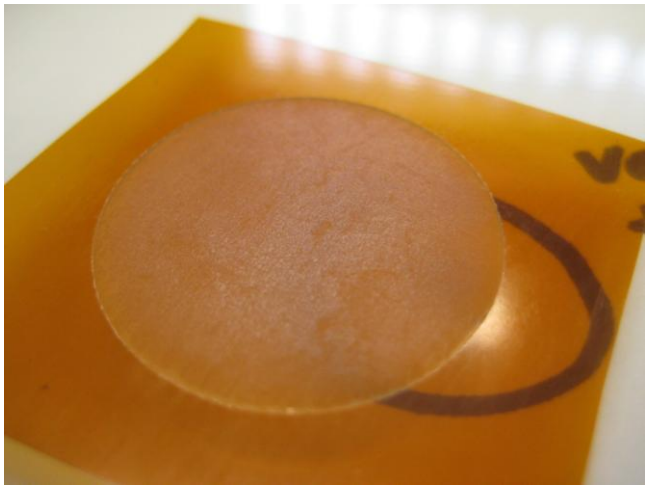

Figure 24. Kapton HN Witness Sample For Second Beta Cloth Test. *There is a noticeable difference in the erosion properties for the Kapton HN witness sample during the second beta cloth test than for any other test, potentially due to contamination of one of the beta cloth samples. The dark markings seen in the photo are simply pen markings underneath a Plexiglass sheet.*

Images using the SEM, shown below in figures 25 and 26 do not show an obvious difference between the exposed and unexposed areas of the second beta cloth test sample. In the left image, a sharp curve can be seen, depicting the edge of the exposure area. On the left of this curve is the exposed area; on the right is the unexposed area. There is no noticeable difference between these two sides, but there appears to be foreign material adhering along the exposure area curve.

Although the first and second beta cloth experiments experienced very different AO fluences, the mass loss of the beta cloth was similar in both cases. This leads to the conclusion that the mass loss of the cloth was not of the beta cloth itself, but of a foreign material on the cloth which was completely eroded away in both cases. The beta cloth itself did not erode. Based on the results of this experiment, it can be concluded that AO+UV exposure will have little effect on spacecraft thermal control with regards to beta cloth.

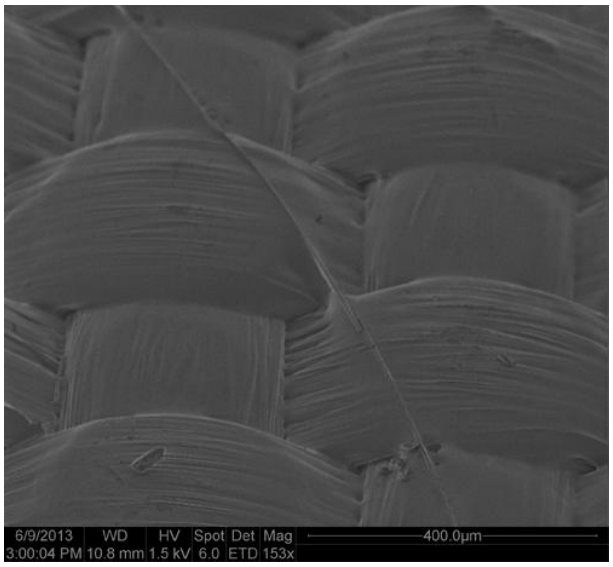

Figure 25. SEM Image of Beta Cloth Exposed to AO+UV – 153x Magnification. *This image depicts the exposed (left half) and unexposed (right half) portions of beta cloth. As can be seen, there is no obvious difference or erosion depth. But, there appears to be foreign material adhering to the beta cloth, along the edge of the exposure area, defined by the sharp curve.*

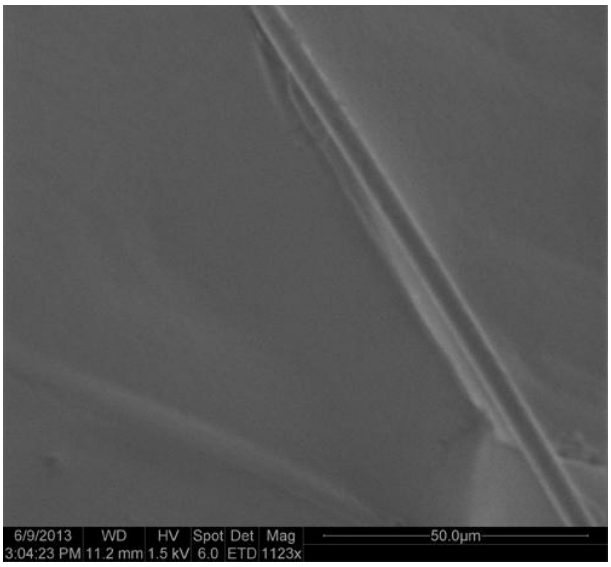

Figure 26. SEM Image of Beta Cloth Exposed to AO+UV – 1123x Magnification. *This SEM image shoes the division between the exposed and unexposed areas with much higher magnification.*

C. Indium-Tin-Oxide Coated Aluminized Kapton

According ground test requirements for the thermal blankets on the Galileo spacecraft, ITO coated surfaces should not be eroded by atomic oxygen, or otherwise stated as atomic oxygen having no visible effects on ITO.[13] ITO is thus used as a protective measure against AO, in addition to being conductive and resisting charge build-up without significantly changing the underlying material's thermal properties.[13] But, the ITO samples used in these tests featured rather significant surface scratches, leading to potentially interesting undercutting effects.

Table 8. ITO – 24 Hour Exposure

No.	Sample Type	Exposure	Avg. Initial Mass (g)	Avg. Final Mass (g)	Average Mass Loss (g)
1	ITO	AO + UV	0.112 ± 0.001	0.111 ± 0.001	0.001 ± 0.002
2	ITO	AO	0.119 ± 0.001	0.122 ± 0.001	-0.003 ± 0.002
3	Kapton 500HN	AO	0.338 ± 0.001	0.315 ± 0.001	0.023 ± 0.002
4	Kapton 500HN	Validation	0.281 ± 0.001	0.261 ± 0.001	0.020 ± 0.002
Mass loss Effective AO Fluence			**ASTM E2089**		$9.2 \pm 2.2 \times 10^{20}$ atom·cm^{-2}
			MISSE 2		$9.8 \pm 2.3 \times 10^{20}$ atom·cm^{-2}

The results of a 24 hour AO and AO+UV exposure are shown in table 8. Although sample #2 featured negative mass loss, the mass loss value is close to zero, barely outside of the margin of error based on the uncertainty analysis described in the analysis section. Different uncertainty analysis may result in the mass loss value being within the bounds of zero mass loss; or, it is possible that the sample received surface contaminants during the test. But, zero mass loss is consistent with the Galileo requirements for ITO-coated thermal blankets. While there was no erosion

depth visible to the naked eye, there was a noticeable discoloration of the exposure area, as can be seen in fig. 26. ITO is a clear material, so the translucent orange of the Kapton layer added to the aluminized backing results in a metallic orange/gold finish for non-exposed ITO. The exposed area of ITO featured a much darker grey hue. There was an especially dark grey hue near the edges of the exposure area, and in specific, seemingly non-random subsections of the exposure area (upper left of the circular exposure area in fig. 26). This dark area may be a sign that the ITO has changed surface properties, or it may be a sign that the underlying Kapton has been partially eroded, especially in the darker areas of the exposure area.

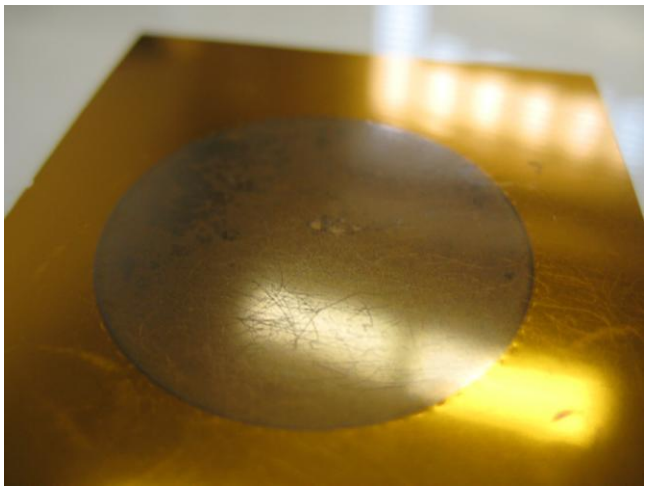

Figure 27. Photograph of an Indium-Tin-Oxide coated Aluminized Kapton Film exposed to AO+UV.

Despite the lack of mass loss, the surface degradation is easily visible in SEM images of the samples. Figures 28 and 29 show the degradation at two different magnifications. At 263x magnification, cracks can be seen adjacent to deep pits. The pits potentially originate as a direct result of the cracks. A crack in the ITO surface would allow AO to contact and react with the underlying Kapton layer. 3386x magnification shows small island-like structures of material either from contaminants piling up on the surface, erosion around surface contaminants, or a combination of both. Even with small or immeasurable mass losses, thermo-optical properties could change significantly. Also, erosion may cause localized weakness in the material which may then lead to eventual rips in the material. For multi-layer thermal blankets, a rip in the outermost layer would result in the exposure of the inner layer to the same harsh environment.

Because the two ITO samples originated from the same sheet, and previous tests using Kapton HN have shown immeasurable synergistic effects due to short test length, the erosion of the AO-only sample is expected to be similar to that of the AO-UV sample. Figure 30 shows a high magnification SEM image of the eroded surface of the AO-only sample. As can be seen in the image, there are similar island-like structures on the surface. Unfortunately, no images of any cracks were taken. But, fig. 31 shows an SEM image of the edge between the exposed and unexposed areas. Small holes can be seen in the diagonal band, possible linked to surface imperfections and a small amount of undercutting. Although the image appears to be showing an erosion depth, this is not the case, especially considering the scale of the image. Based on the fact that erosion depth of the Kapton HN samples could easily be seen with the naked eye, but the SEM images were on a much smaller scale, an erosion depth this large would easily be seen by the naked eye. The diagonal band in fig. 30 may originate due to a shadowing effect of the polished aluminum sample containment plate, which has a finite thickness. Near the edges of the exposure area, the “wall” of the hole cutout on the polished aluminum plate would block a portion of the incoming AO atoms by nature of the non-directional, isotropic plasma.

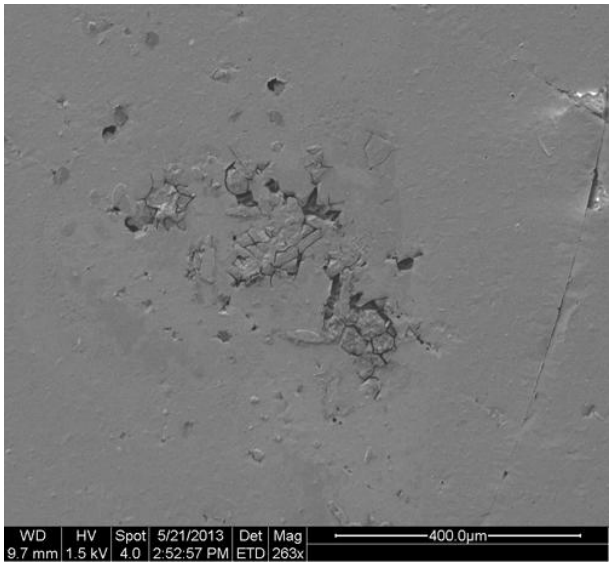

Figure 28. SEM Image of ITO Coated Aluminized Kapton Exposed to AO+UV – 263x Magnification. *Surface imperfections in the ITO coating may have lead to cracks and undercutting caused by AO+UV erosion.*

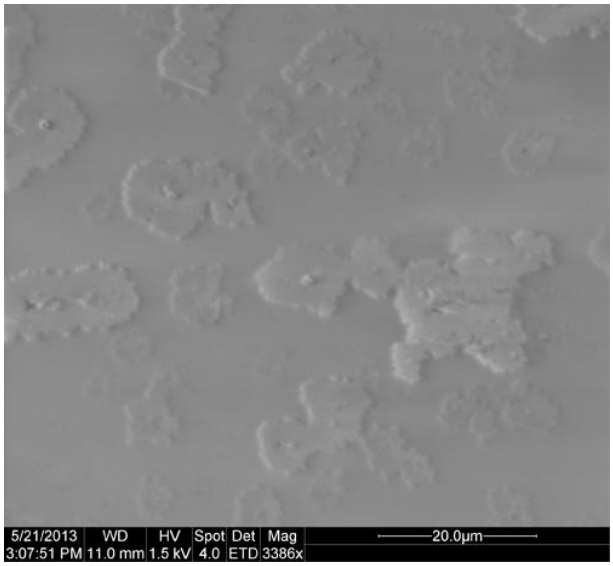

Figure 29. SEM Image of ITO Coated Aluminized Kapton Exposed to AO+UV – 3386x Magnification. *High magnification reveals island-like structures on the surface of the exposed area. These structures are potentially formed by the buildup of contaminants, or by the protection of underlying material by contaminants.*

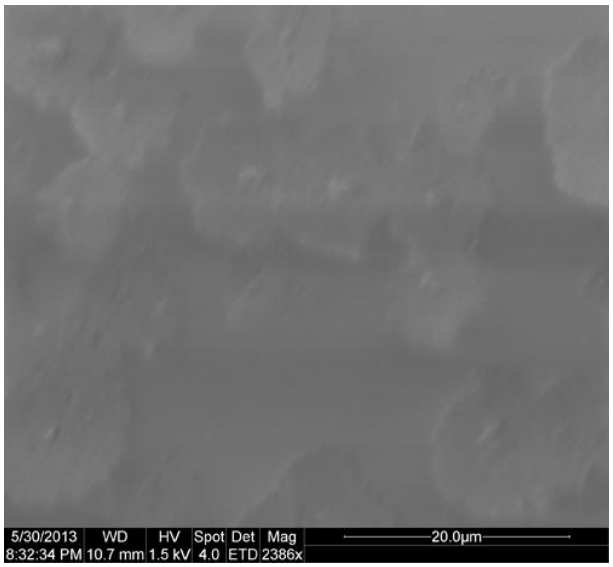

Figure 30. SEM Image of ITO Coated Aluminized Kapton Exposed to AO – 2386x Magnification. *High magnification reveals similar island-liked structure on the AO-only ITO samples.*

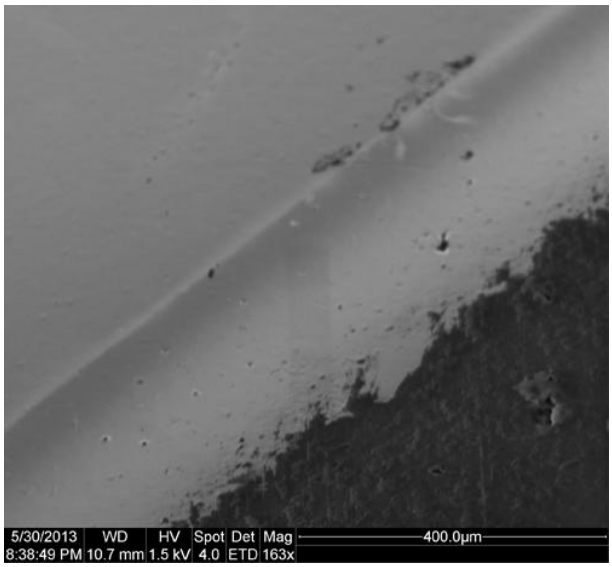

Figure 31. SEM Image of ITO Coated Aluminized Kapton Exposed to AO – 163x Magnification. *Small pits potentially originate from surface imperfections, leading to undercutting. The diagonal band across the imagine should not be misinterpreted as an erosion depth, especially considering the scale of this image. It is believed that this band is caused by shadowing of the exposure area from AO.*

The change in surface properties can be seen by observing the change in the reflectance of the surface. Even with the naked eye, a noticeable difference in the reflectance could be seen due to the discoloration of the ITO surface, which is clear in its non-degraded state. A plot of the reflectance before and after AO+UV exposure is shown in fig. 32. It can easily be seen that the unexposed ITO coated aluminized Kapton has a low reflectance. This is due to the

highly reflective nature of the aluminized Kapton, which acts as a second mirror. After exposure, there was a significant increase in reflectance, indicating that the material was not fully functional as a protected second surface mirror as was expected of the material (without surface imperfections). There was an average diffuseness increase of 181% across the 350-2500 nm wavelength range. Specifically, there was a large increase in the infrared region, which extends from 700nm to 1mm, signifying that the second surface mirror reflects much less infrared light energy after exposure than before exposure. Similar to the Kapton HN samples, this would result in increased spacecraft temperatures.

Failure of the ITO coating to resist AO corrosion not only has thermal implications due to changed thermo-optical properties, but also electrical implications. ITO is often used to bleed off electrical charge that may accumulate on the surface of thermal blankets.[8] Partial or complete erosion of the ITO coating would result in a decreased ability to bleed off this electrical charge.

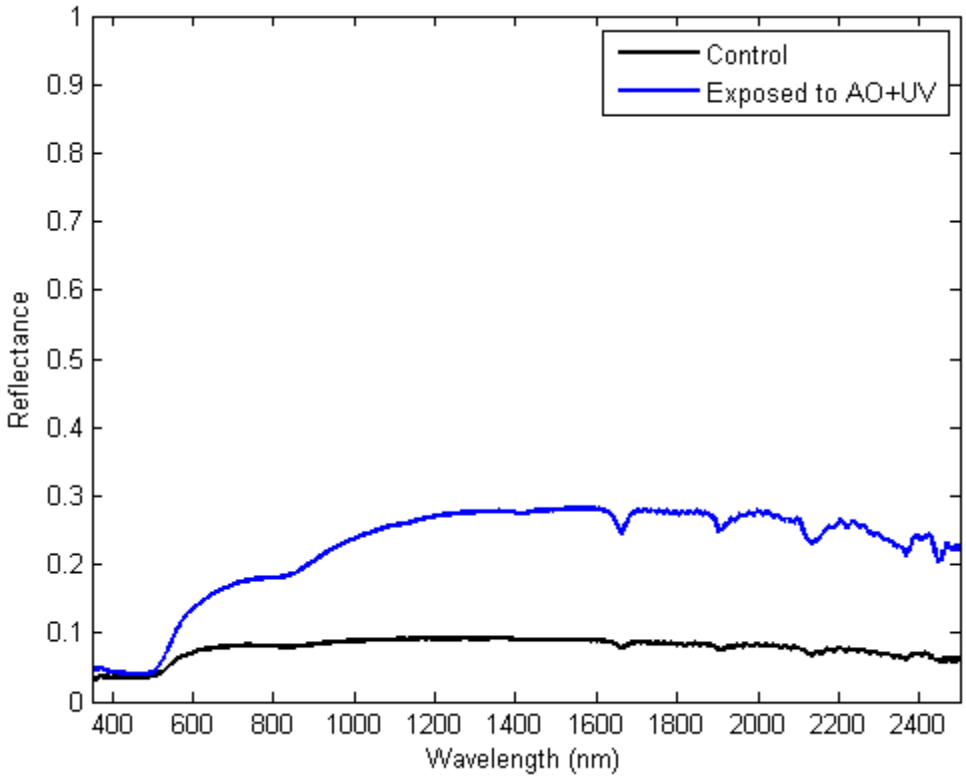

Figure 32. ITO Reflectance Before and After AO+UV Exposure.

VI. Conclusion

Several tests were performed to validate the AOSS and UVRS, including a 24 hour and 12 hour test using Kapton HN witness samples. Ideally, a significant difference in erosion characteristics between simultaneous AO and UV exposure, and single AO exposure would be encountered upon completion of these tests. The lack of a noticeable difference in mass loss and reflectance outside the margins of error indicates that the test durations were too short to realize any increased synergistic effects. Future tests should be performed using much longer test durations, such as 48 or more in order to better simulate the space environment. However, the potential for the occurrence of reflected RF power in the system necessitates almost constant monitoring of the RF system parameters. These extended length tests can be difficult to monitor in-person, even by several students. A webcam system or a means of obtaining the system parameters digitally from the Seren RF components would ease the monitoring process.

Should longer test durations be implemented, then the gap distance and forward power may be adjusted in order to lower the AO flux to better match the VUV flux. As is currently designed, a single test 24 hour test yields equivalent LEO AO fluences of several months, while only yielding several days in equivalent sun power. Lowering the AO flux would thus better match the LEO environment, although this would also require longer test durations in order to achieve the same AO fluences.

Exposure of beta cloth to AO and UV yielded expected results; though, contamination was likely present in the system during the second of the two beta cloth tests. Surprisingly, the ITO coated aluminized Kapton featured significant surface degradation, despite no measurable mass loss. Because the ITO coated aluminized Kapton donated by Sheldahl was space-rated, it should not have seen a noticeable degradation. The degradation is possibly due to surface scratches and imperfections. Future tests should reexamine beta cloth and ITO samples while avoiding contamination and scratching of the material surfaces. In addition to reflectance, the absorptance and emittance of the materials before and after exposure should be analyzed. Because ITO coatings function to bleed off electrical charge, the change in surface resistance across the ITO surface should be recorded. Additionally, various other materials donated by Sheldahl should be tested. Although reflectance was measured for some samples, measuring of the thermal effective emissivity and absorptance would result in increased understanding of the effects of atomic oxygen and UV degradation on thermal materials.

Appendix

A. Lessons Learned - Overall

The first lesson learned is that schedules are very important not only to create, but to follow. Test schedules can easily fall behind when unexpected technical difficulties arise. If everything works 100% as it should, it is most likely a fluke. And no, "fluke" does not refer to the manufacturer of yellow digital voltmeters. All jokes aside, time margin should be allocated to allow for inevitable mistakes and or failures. When problems do arise, the problem should be discussed with all of those directly involved in the matter so that a solution can be found as quickly as possible. Do not be afraid to contact those whom are extremely knowledgeable in the subject. If there were never any problems, then there would be no such thing as engineering.

The second lesson learned is that requirements should be clearly defined, both by the student completing the project him/herself, and for others contributing in some way to the project. When interfacing with other departments or students, requirements should be clearly and explicitly explained and produced in writing. Any misunderstandings should be discussed immediately.

The third lesson learned is that extensive research is good – but students should not be afraid to start because they cannot find all of the answers in databases. Halting the start of a project to complete excessive research will result in further delays. That being said, projects should not be started without any research completed. Additionally, information should be researched through the entirety of the project, even up until the end. Although projects need to be completed by deadlines, ignorance of helpful information that either reinforces or contradicts an experiment's results because of a looming deadline is detrimental to the learning philosophy.

The fourth lesson learned is that tripods are ideal for setting the angle of a surface, while four points of contact makes overall angles very difficult to adjust. As opposed to adjustment of the four posts on the sample containment plate in a random order, the angle should be adjusted first from side to side, and then from front to back. Use a level at multiple locations on the dark space shield and the sample containment plate in order to verify that they are parallel with each other. It is important to ensure that all samples are an equal distance from the RF electrode.

B. Lessons Learned – Fixing the MAX chamber and AOSS

The golden rule to having the AOSS work smoothly and properly is: When in doubt, use more tape. Lack of sufficient layers of aluminum tape was the source of many problems during this experiment. Reflected RF power would not be mitigated for weeks while a solution was brainstormed. More often than not, the proper mitigation procedure was to add more aluminum tape.

If reflected RF power unexpectedly occurs, attempt to reduce the reflected power back down to 0W using the tuning functions on the Seren MC2 Controller. If the reflected power cannot be reduced to 0W within several minutes, abandon the experiment and turn off the RF power. First, consider any recent changes that may have been made to the chamber or AOSS. The system is extremely finicky, and even small changes can result in the occurrence of reflected power. Ensure that all electrical connections are making intimate contact with whatever they are attached to. Then, inspect the cleanliness of the copper grounding straps. If they appear to be dirty or oxidizing, remove the straps and place them in a bag with a shallow pool of vinegar at the bottom (this saves vinegar, as opposed to using a large container and filling it completely). Let the first surface of the ground strap soak in the vinegar for at least a few minutes, then rotate and continue until all the surfaces are clean. If vinegar alone is not sufficient to clean the ground straps, then fine-grit wet-sandpaper may be used simultaneously with the vinegar.

Next, inspect the quality of the tape work on all of the RF lines. This includes both the Kapton tape, as well as the aluminum tape. Ripping off all of the tape is both time consuming and wasteful, but sometimes it must be done. If no other problems can be found, remove all of the tape and check that all coaxial electrical connections are secure.

The #10 screw and nut connected the RG393 cable to the feedthrough both inside and outside of the chamber often comes loose. Do not forget to inspect the quality of the electrical lines themselves. For example, it was found that the RG393 cable was beginning to fray from the ring connector, after months of movement. The joint was re-soldered and enforced to ensure that it would not move or break in the future.

If changes to the system must be made, try to document the changes one at a time and test each change before moving on to another. This will help when backtracking changes to find the potential source of a problem. RF power is very finicky, and occasionally there will be no logical solution to the problem. After resolving the power of reflected power, even turning the system completely off and back on would result in the reoccurrence of reflected power. Occasionally, manual system tuning using the Seren MC2 is required to mitigate the problem, even though the MC2 and AT3 Matching Network are designed to automatically match system impedance.

Acknowledgments

The author would like to thank Dr. Kira Abercromby for her advisement on this senior project and for her procurement of reflectance data using the spectrometer. The author would also like to thanks Max Glicklin for his help with the MAX, AOSS, and UVRS apparatuses and understanding of key concepts, and Eli Gurnee for his help with magically finding the tuning combinations in order to mitigate reflected power. Furthermore, the author would like to thank Dr. Trevor Harding and the Cal Poly Materials Engineering Department for procuring the SEM images. Additional thanks go to Isaac Nitschke for his provision of loud and amusing rants in the lab, Matthew Stumbo for his use of bad (but humorous) puns, and Dr. Kira Abercromby again for putting up with the endless banter of the Space Environments lab technicians.

References

[1]Tribble, A. C., *The Space Environment, Implications for Spacecraft Design*, Revised and Expanded Edition, Princeton University Press, New Jersey, 2003.

[2]Pisacane, V.L., *The Space Environment and Its Effects on Space Systems*, AIAA Education Series, AIAA, Virginia, 2008, Chap. 7.

[3]Banks, B., Backus, J., and de Groh, K. K., "Atomic Oxygen Erosion Yield Predictive Tool for Spacecraft Polymers in Low Earth Orbit," NASA TM-215490, 2008.

[4]Glicklin, M., "Development of a Ground Based Atomic Oxygen and Vacuum Ultraviolet Radiation Simulation Apparatus," M.S. Thesis, Aerospace Engineering Dept., California Polytechnic State University, San Luis Obispo, CA, 2012.

[5]"Standard Practices for Ground Laboratory Atomic Oxygen Interaction Evaluation of Materials for Space Applications," ASTM E2089-00, American Society for Testing and Materials, 2006.

[6]Minton, T. K., "Protocol for Atomic Oxygen Testing of Materials in Ground-Based Facilities," Version No. 2, JPL Publication 95-17, 1995.

[7]"S2D2 VUV Light Source Unit – L10706 Series," Product Brochure, TLSZ1001E02, Hamamatsu Photonics K.K., August 2011.

[8]"The Red Book," Sheldahl, PB-1007, Rev-A.

[9]Banks, B., de Groh, K. K., et al, "MISSE PEACE Polymers Atomic Oxygen Erosion Results," NASA TM-214482, 2006.

[10]"DuPont Kapton – polyimide film," Product Brochure, H-38479-9, DuPont, March 2012.

[11]Shimamura, H., and Miyazaki, E., "Investigations into Synergistic Effects of Atomic Oxygen and Vacuum Ultraviolet," *Journal of Spacecraft and Rockets*, Vol. 46, No. 2, March-April 2009, pp. 241 – 247.

[12]Kamenetzky, R. R., and Finckenor, M. M., "MSFC Investigations of Beta Cloth Darkening Due to Ultraviolet Radiation Interactions," Marshall Space Flight Center, 1999.

[13]Bouquet, F. L., and Maag, C. R., "Ground Radiation Tests and Flight Atomic Oxygen Tests of ITO Protective Coatings for Galileo Spacecrat," *IEEE Transactions on Nuclear Science*, Vol. NS-33, No. 6, December 1986, pp. 1408-1423.